CHALMERS

Bismuth-containing multiferroics; *Synthesis, structure and magnetic properties*

Master of Science Thesis in the Masters Degree Programme Materials and Nanotechnology

Shengzhen Cai

Department of Chemical and Biological Engineering

Division of Energy and Materials

CHALMERS UNIVERSITY OF TECHNOLOGY

Gothenburg, Sweden, 2013

Abstract

Materials that combine multiple ferroic properties, such as ferromagnetism, ferroelectricity and ferroelasticity, are defined as multiferroics. Attempt to reduce the electrical leakage, enhance the magnetoelectric property as well as stabilize the formed multiferroics $BiFeO_3$ was made by adding various dopants or forming solid solution with other compounds.

Conventional solid state method was adopted to synthesize the $xBiFeO_3$-$(1-x)SrTiO_3$ ($0.1 \leq x \leq 0.7$).X-ray diffraction data indicated a stabilized cubic structure up to x=0.6, above which a structural phase transition towards a rhombohedral R3c emerged. As more $BiFeO_3$ incorporated, the magnetic property of $xBiFeO_3$-$(1-x)SrTiO_3$ shows a conversion from paramagnetism to antiferromagnetism with trace amount of ferromagnetism.

In addition to the $xBiFeO_3$-$(1-x)SrTiO_3$, coprecipitation route was chosen to prepare $Bi_{1-x}La_xFeO_3$ ($0 \leq x \leq 0.2$) and $Bi_{1-x}Tb_xFeO_3$ ($0 \leq x \leq 0.2$). Thermal analysis was performed on the powdered $Bi_{1-x}La_xFeO_3$ by means of DSC. In comparison with the Curie temperature, the Neel temperature is less sensitive to the compositional change. Meanwhile, the structures of $Bi_{1-x}La_xFeO_3$ ($0 \leq x \leq 0.2$) and $Bi_{1-x}Tb_xFeO_3$ ($0 \leq x \leq 0.2$) were characterized by XRD. Depending on the concentration of substituted elements and the ionic size difference among Tb^{3+}, La^{3+} and Bi^{3+}, the $PbZrO_3$-type Pbam structure is only stable in the phase transformation of the lanthanum substituted bismuth ferrite.

Table of Contents

1. Introduction

1.1 Aim of this project

Motivated by the previous investigations of multiferroic material bismuth ferrite, it stimulates further efforts to synthesize binary perovskite solution $xBiFeO_3$-$(1-x)SrTiO_3$ as well as the isovalently substituted $BiFeO_3$, i.e. $Bi_{1-x}La_xFeO_3(0\leq x\leq 0.2)$ and $Bi_{1-x}Tb_xFeO_3(0\leq x\leq 0.2)$ in order to track their phase transformations at different compositions and develop different synthesis methods that can curb the formation of impurity phases.

The purpose of this research study was to strengthen understanding about solid state chemistry and to familiarized with different synthesis methods and various characterization techniques, e.g. calorimetric, gravimetric and diffraction techniques.

1.2 Ferroic properties and multiferroics

Ferro- is a prefix which means iron in Latin, it is primitively used to describe materials exhibiting strong magnetic properties as iron does. Apart from iron, other elements like cobalt, nickel and rare earth elements also exhibit magnetic behavior called ferromagnetism, which enables materials made from the above-mentioned elements to form permanent magnets.

Ferromagnetic materials were reported to have a long-range ordering phenomenon at the atomic level. Many small domains can be found in a magnetic material with plenty of unpaired electrons inside. Microscopically, those unpaired electrons are not randomly aligned, they interact with others to make the alignment in the same direction within the same domain. However, these domains are randomly aligned so that on the whole, they cancel out to make zero magnetism.

When an external magnetic field is applied, those domains with the magnetic field grow at the expense of their neighboring domains, causing materials to be magnetized. This phenomenon is characterized by a hysteresis loop of magnetization M as a function of external magnetic field H, as illustrated in Figure 1.1 (a). It is obvious that the magnetization is saturated at high magnetic field and a remnant magnetization can still exist in the absence of the field. In addition, the direction of magnetization could be reversed provided that the external

magnetic field is switched oppositely with quite strong field intensity.

However, the ferromagnetic material can lose its ferromagnetic properties under thermal agitation, the temperature that characterizes this phenomenon is known as the “Curie temperature (Tc)”, above which spontaneous ferromagnetism becomes paramagnetism which owns a small, positive susceptibility to magnetic fields and can’t keep this magnetic properties after removal of the external field.

Ferroelectricity and ferroelasticity are analogous to ferromagnetism. Polarization and strain are induced by externally applied electric field and mechanical stress respectively. They both show hysteresis loops with spontaneous electric polarization and strain, as depicted in Figure 1.1 (b) and (c).

Actually, the discovery of ferroelectricity can date back to the early 20th century when ferromagnetismhad already been discovered. Since the appearance of hysteresis loops from ferroelectricity and ferromagnetism look quite similar, the prefix ferro- was continuously carried forward to describe ferroelectricity, though many ferroelectric materials have nothing to do with iron either.

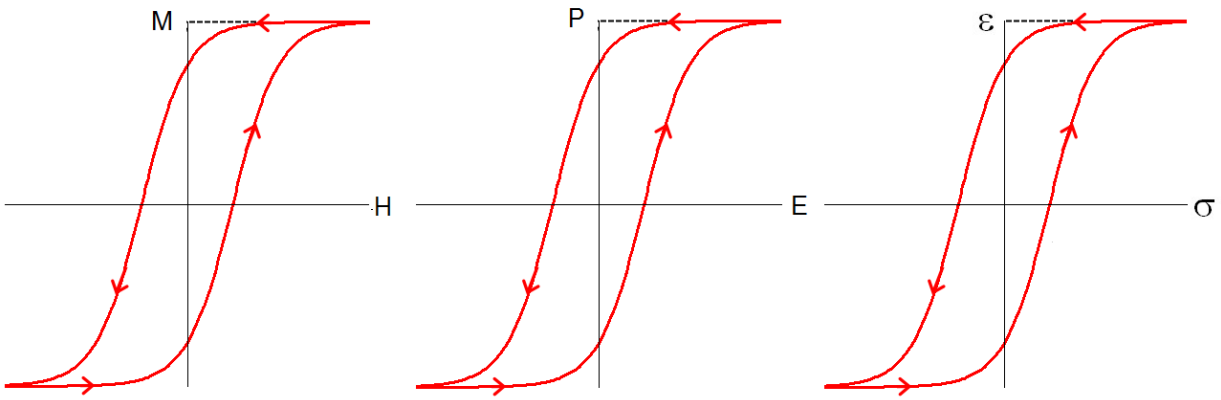

Figure 1.1 Hysteresis loops of (a) ferromagnetic, (b) ferroelectric and (c) ferroelastic materials.

Multiferroics

The simultaneous coexistence of at least two ferroic properties, (anti)ferromagnetism, (anti)ferroelectricity and (anti)ferroelasticity in the same phase is defined as multiferroics, as shown in Figure 1.2. These materials have the potential of exhibiting coupling between ferroelectricity and magnetism, known as the magnetoelectric effect, which enables the external electric field to change magnetization and vice versa.

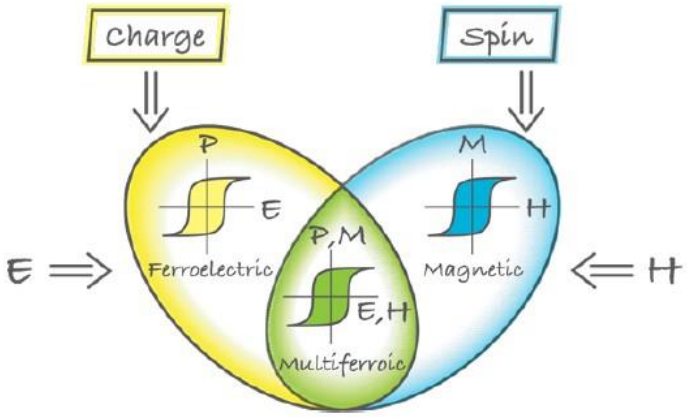

Figure 1.2 Schematic illustration of multiferroic defined from the overlap region of ferroelectric and magnetic.[5]

However, looking back in history, the combination and correlation of magnetism and electricity were well interpreted by Maxwell equations in the 19th century, but magnetic and electric ordering in solids were always treated separately at that time. This is because the magnetic properties were understood to be attributed to the spin of electrons while the electric properties resulted from the electric charges of ions and electrons.

This situation changed after the hypothesis was proved to be untrue. The preliminary proposal of the magnetoelectric effect was made in 1894 by Curie indicating that an asymmetric molecular body can be polarized by a magnetic field. Later in 1960, Dzyaloshinskii[1] predicted the magnetoelectric effect in antiferromagnetic Cr_2O_3 and in the meantime, Astrov[2] also observed this coupling by measuring the electric field-induced magnetization. The magnetic field induced-electric polarization was also studied by Folen et al.[3] in 1961.

Nowadays, the coexistence of ferroelectricity and magnetism attracts a great deal of attention. The potential application of multiferroics is quite extensive and promising, ranging from giant electric transformers to a small computer memory devices or even tiny sensors.[4] Unfortunately, most of the multiferroics are not naturally-occurring materials and fewer materials possess magnetoelectric properties. Majority of multiferroic materials have low magnetic ordering and ferroelectric transition temperature. This can be partly improved by introducing dopants (such as rare-earth elements) into the original material. Moreover, since the microscopic origin of magnetism can be described as the presence of localized electrons, mainly in the partially filled d or f shell of transition metals or rare-earth ions having a corresponding localized spin. By contrast, ferroelectric materials require transition metal ion with an empty d shell, and the displacement of such transition metal ion towards an apical atom (normally oxygen) creates electric diploes that are stabilized by the strong covalent

bonds between O 2p and empty d orbitals. The mutual exclusion of ferroelectricity and magnetism give rise to a problem called "d^0 versus d^n". In order for the coexistence of magnetism and ferroelectricity to occur, both the elements and structures need to be considered. In the perovskite type structure (ABO_3) multiferroics, the A site element is selected to take the responsibility for the ferroelectricity while the element at the B site accounts for the magnetism. For instance in the perovskite $BiMnO_3$, the $6s^2$ lone pair of Bi^{3+} tends to hybridize with O 2p orbital, which improves the ferroelectricity by driving the Bi^{3+} towards the oxygen ions, while the Mn cation has non-zero d-electrons.

What is more, the geometric change from tilting of rigid blocks can improve ferroelectric properties as well. Taking $YMnO_3$ for example, to get closer packing the MnO_5 block is rearranged through a small tilting. As a consequence of this tilting, the indicated oxygen ions move close to the indicated Y ions and the Y-O bonds form dipoles with two dipoles up and one dipole down in one block, resulting in polarizations in $YMnO_3$, as illustrated in Figure 1.3.

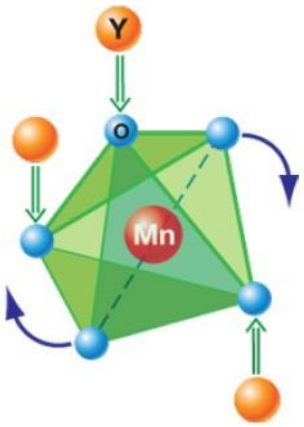

Figure 1.3 Polarization caused by the titling of MnO_5 in $YMnO_3$.[5]

1.3 Tilted octahedra in perovskite

Perovskites structure attracts considerably attention currently. These perovskites often exhibit properties like ferromagnetism, ferroelectricity or/and piezoelectricity. The generic formula for the perovskite is ABX_3, which consists of an array of corner-linked octahedra with B-cation placed in the center surrounded by six X-anions (usually oxygen or fluorine atom). The A-cation is positioned in the interstices surrounded by eight B-cations and twelve X-anions. Figure 1.4 illustrates a typical perovskite structure of $SrTiO_3$, the red dots are oxygen representing X in the formula while the B site and A site ions are shaded blue and orange, which are occupied by the atoms of titanium and strontium respectively.

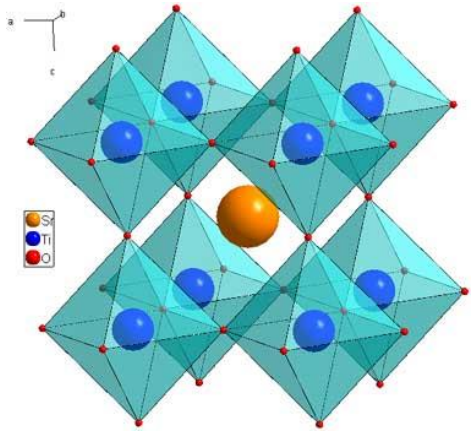

Figure 1.4 Stereo illustration of B-cell octahedral framework of perovskite $SrTiO_3$.

In fact, perovskite can be viewed from different perspectives. The stereo picture presented above is a B-cell setting with B-site at the origin and A-site in the center of eight octahedra. However, A-cell setting is also exist and preferred in some cases, where perovskite is originated from A-site and making B-site positioned at the center of the cell (see Figure 1.5).

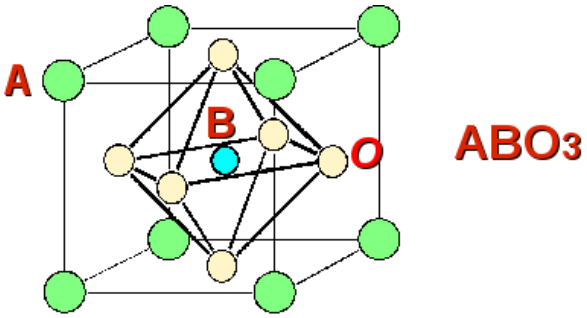

Figure 1.5 Perovskite structure of A-cell setting with B-site positioned at the center of the unit cell..

For materials with perovskite structures, it can be an ideal structure without any tiltings and distortions, like $SrTiO_3$ depicted in Figure 1.4 at room temperature. However, under certain conditions, structures with ion displacement or/and octahedral tilting might take place, which could change their original symmetry and unit cell parameters.

The octahedra can be tilted in various ways, which influences their neighbours and changes the whole crystal symmetry. In order to fully understand the changes of structures, a logical interpretation has been proposed by A.M.Glazer in 1972[6]. He divided the overall tilts according to the three axes ([100], [010] and [001]) and three letters were chosen to indicate the magnitudes of tilting along the three axes. Superscripts + or – were adopted to show whether the successive octahedral tilting is in the same direction (+) or in opposite direction (-) or

even without moving (0). Unequal tilts are denoted by different letters while equal tilts are characterized by the same letter, 0 means no tilts at all along that axis. For instance, $a^0b^+c^-$ indicates unequal tilts occur along the axes of [010] and [001] but no tilts along the axis [100]. The octahedral pair along [010] axis tilt towards the same direction while they are tilted in the opposite way along the axis [001]. Stereo photographs of octahedra before and after tilting are shown in Figure 1.6.

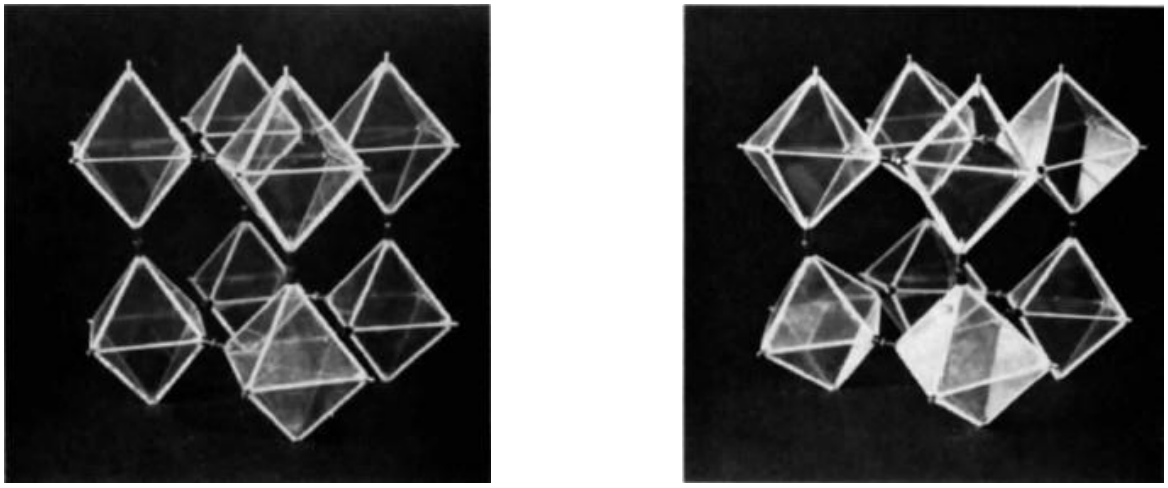

Figure 1.6 Stereo-photographs of octahedra a^0 a^0 a^0 without tilting (left) and after tilting $a^0b^+c^-$ (right).

1.4 $BiFeO_3$

Bismuth ferrite ($BiFeO_3$) is one of the few multiferroics that has Curie and Neel temperatures above room temperature. Magnetoelectric coupling is realized at room temperature and such coupling is strongly enhanced by proper dopings.[7]

$BiFeO_3$ is a typical multiferroic material that has been extensively investigated nowadays. The initial research on $BiFeO_3$ was carried out by Smolenskii in 1960.[8] But at that time, they were not able to make single-phase polycrystalline $BiFeO_3$ and the $BiFeO_3$ produced was not stable for practical application. In 1967, Achenbach successfully prepared single-phase $BiFeO_3$ by removing the undesirable phases using HNO_3.[9] X-ray diffraction technique was also adopted to investigate the monodomain single-phase by Kubel and Schmid in 1990.[10] Later in 2003, Ramesh and his colleagues produced thin film $BiFeO_3$ which exhibited remnant polarization 15 times stronger than that of the bulk $BiFeO_3$.[11] It has also been reported that the low symmetry monoclinic or tetragonal thin film $BiFeO_3$ might be the origins of strong polarization.[12, 13] Until recently, increasing efforts have also been devoted to the research focusing on the preparation and characterization of $BiFeO_3$ in forms of

film, bulk and nanostructure.[14, 15]

Single phase $BiFeO_3$ has rhombohedrally distorted perovskite structure R3c with antiphase rotation of FeO_6 octahedra by 12°, denoted as $a^-a^-a^-$ in the Glazer notation. The displacement of the A-site bismuth cation along the [111] pseudo-cubic axis brings about a non-centrosymmetric polarization resulting in the ferroelectric property. The actual structure of $BiFeO_3$ can be understood by an imaginary structural transition process, as shown in Figure 1.7. The lattice parameters for bismuth ferrite with rhombohedral structure are 3.965Å and 89.4°[16] or a=5.58 Å and c=13.9 Å if viewed in the hexagonal setting at room temperature.[17]

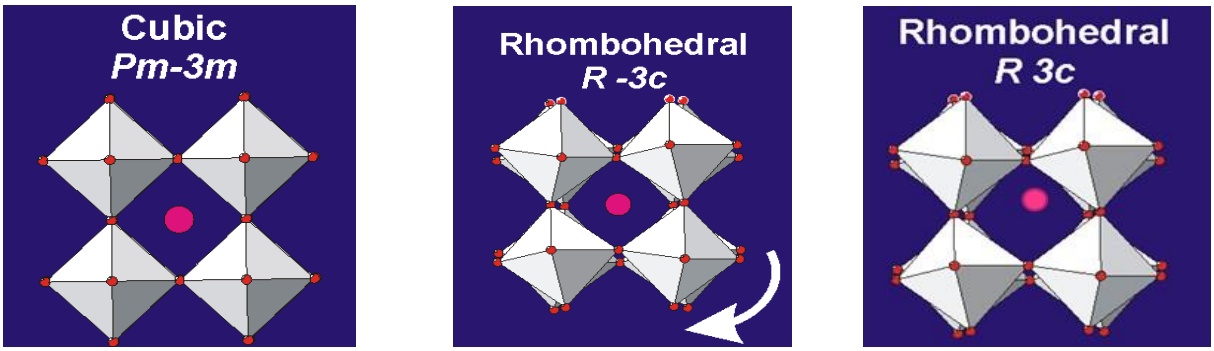

(a) (b) (c)

Figure 1.7 Schematic illustration of a structural transition process **(a)** ideal cubic structure Pm-3m without tilting ($a^0a^0a^0$) ; **(b)** R-3c structure tilted along three axes with the same angle ($a^-a^-a^-$) ; **(c)** Displacement of Bi ion towards [111] direction based on R-3c.

The lattice parameter and crystal structure of $BiFeO_3$ are dependent on the temperature. The atomic coordination are slight changed between 5K and 300K. Significant changes are observed above 300K, the influence of temperature on the cell parameter, volume, bond distance and bond angle are shown below in Figure 1.8.

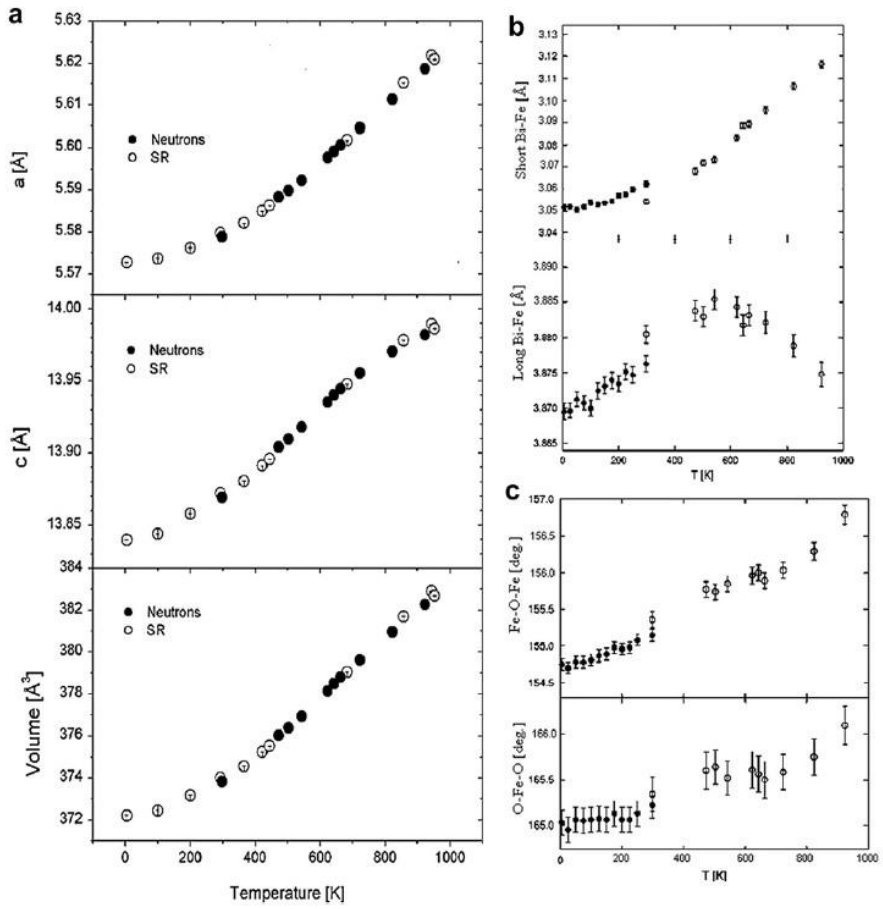

Figure 1.8 Plots of temperature (0-1000K) as functions of (a) lattice parameter a, c and volume of $BiFeO_3$ (b) short and long distance of Bi-Fe bond (c) Fe-O-Fe and O-Fe-O angles.[18]

It was well documented that, except for the long Bi-Fe bond distance, the lattice parameter a, c, the volume of unit cell, the short bond distance of Bi-Fe as well as the bond angles gradually increase with increase in temperature. As a consequence of these variations, magnetism and polarization are reported to be gradually reduced, and structural phase transitions are also induced from the rhombohedrally distorted R3c perovskite structure to an orthorhombic Pnma structure at 1098K and eventually to a cubic structure above 1204K.[19]

However, single phase $BiFeO_3$ is difficult to synthesize. Due to the metastable nature of bismuth ferrite in air[20] as well as the volatility of bismuth oxide, their stoichiometry can be changed resulting in impurities of Bi_2O_3, $Bi_{25}FeO_{39}$ and Bi_2FeO_9 during the sintering process. The phase diagram of Fe_2O_3 and Bi_2O_3 is presented below in Figure 1.9 [20], unequal amount of Fe_2O_3 and Bi_2O_3 is seen to bring about impurity phases $Bi_{25}FeO_{39}$ (bismuth-rich) and Bi_2FeO_9 (bismuth-deficient).

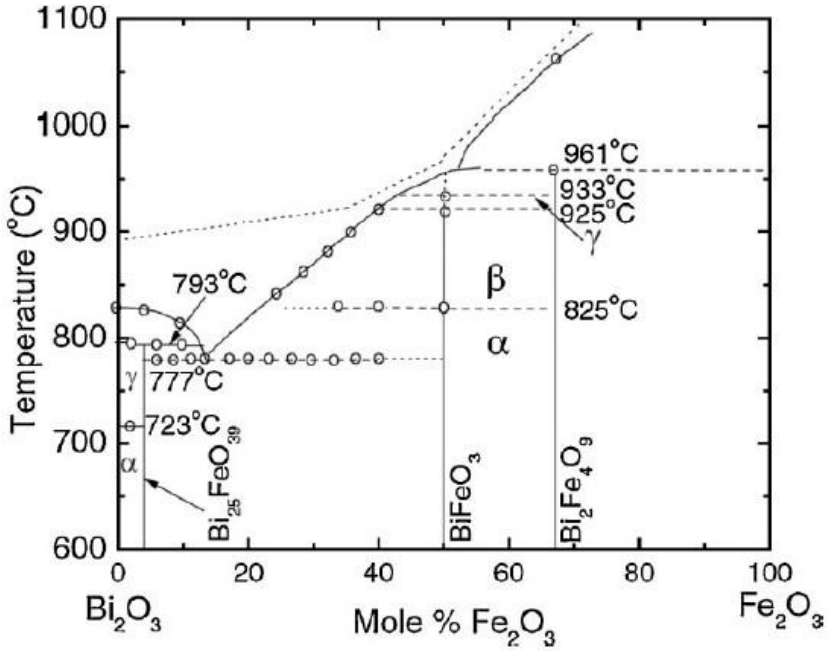

Figure 1.9 Phase diagram of Fe_2O_3 and Bi_2O_3 showing bismuth ferrite with undesired impurities.

2. Techniques used in the project

2.1 PXRD

X-rays are a type of electromagnetic radiation. The wavelength of x-rays is approximately 1 Å which has the same size equivalent to that of an atom. Powder X-ray diffraction (PXRD) is a non-destructive analytical technique mainly used for the phase identification and structural characterization of crystalline materials. Powder X-ray diffraction combined with Rietveld analysis, provides detailed information regarding unit cell dimensions, bond-lengths, bond-angles and the site ordering of crystallites.

The relationship between the wavelengths of the X-rays λ, the incidence angle θ, and spacing between two crystal lattice planes (hkl) d, is shown in the Bragg's Law expressed as:

$$2d_{hkl}\sin\theta = \lambda \tag{1}$$

After characterization by Powder X-ray diffraction, a number of peaks are seen in the diffraction patterns. These patterns are identified by comparing their positions and relative intensities with the known structures in the database (such as database developed by the International Center for Diffraction Data). Sometimes extra peaks might appear due to the impurity or structural transformation after thermal treatment. In fact, the intensities, widths and positions of peaks in the patterns reflect information about structure, quantity, texture etc. of crystallites. Almost all the factors are linked to certain parameters that can be refined by computer programs.

Rietveld Refinement

Rietveld Refinement is a method used to determine detailed information of crystalline materials. In order to get authentic information about crystalline materials, the least square value of the difference between theoretical and experimental peak intensities are supposed to be minimized based on releasing and refining appropriate parameters, as shown below in equation (2),

$$X^2 = \sum_i w_i \left(I_i^{exp} - I_i^{cal}\right)^2, \quad w_i = \frac{1}{I_i^{exp}} \tag{2}$$

where χ is the least square, I represents intensities of calculated and experimental peaks.

Rieveld Refinement directly matches the intensities of all the peaks throughout the test range with the intensities of peaks from the model structures, and it is less sensitive to both model and experimental errors. However, to get more accurate information about crystalline materials, a wide range 2φ of experimental pattern and good models in database are needed. In addition, the experience of operating the Rietveld programs is quite necessary along with a good chemical knowledge in terms of expected bond distances.

Many computer programs can be selected to conduct the refinement work, such as GSAS, Maud, Fullprof, etc. The most popular one is the GSAS-Expgui which has also been chosen for the Rieveld Refinement in this work. In this thesis work, powder state samples were characterized by Bruker D8 Advance X-ray powder diffraction (Cu-Kα_1, λ = 1.54056 Å).

Figure 2.1 Bruker D8 Advance PXRD instrument.

The applications of x-ray power diffraction technique are quite extensive, ranging from polymers, ceramics to minerals and metals. In general, information regarding structure determination, crystal orientation (texture) and phase composition in a quantitative and qualitative way can be obtained by diffraction techniques with the help of some professional softwares.

2.2 Thermal Analysis

Detail information regarding mass changes and caloric effects of a specimen during heating and cooling process can be measured simultaneously by means of TG-DSC Netzsch STA 409 PC Luxx analyser. A plot of mass change and heat flow as a function of temperature can be obtained in one graph upon heating and cooling.

There is a highly sensitive balance with two identical crucibles placed on both sides, one of which serves as a reference that should keep always empty and clean. Before performing the thermal analysis, the instrument is supposed to be calibrated by making two empty crucibles balanced first. After filling one of the crucibles with the test sample, a gradual heating process is introduced inside the chamber with gas flow at certain speed. Before getting an reliable experimental result, a baseline correction is required by subtracting the empty crucible run from the original sample run.

The purpose of using this thermal analysis is to specify the water of hydration in the reagents of nitrates for the solution synthesis and to determine the antiferromagnetic ordering temperature T_N and ferroelectric temperature T_c.

2.3 Magnetization measurement

Magnetization measurements were conducted at Uppsala University on a Quantum Design SQUID MPMS XL magnetometer. Thanks to Roland Mathieu, the magnetic measurements were performed on the system of $xBiFeO_3$-(1-x) $SrTiO_3$ with x=0.1, 0.2, 0.3, 0.4, 0.5, 0.6 and 0.7, where magnetization *M* was measured as a function of applied field *H* at only 5 K.

2.4 Calcination and sintering

The conventional solid state synthesis route, also known as the ceramic method, refers to a procedure of heating two or more non-volatile solid state materials that can react with one another forming a new compound.

Typically, the high temperature treatment (500°C-2000°C) is required during the process, which provides the energy condition that enables the ions to leave their original sites and diffuse to different sites. The solid state reaction is quite slow but the reaction can speed up considerably if the temperature is increased. However, due

to the decomposition or melting of materials, extremely high temperature is not favored. In principal, the optimal temperature is defined by a rule of thumb that two-thirds of the melting temperature of the compound always gives best reaction time.

The solid state reactions are always performed in either box furnace or tube furnace, high resistances of metal heating elements inside the furnaces create heat by conversion of electrical energy. In general the tube furnace can withstand higher temperatures (<2300°C) than that of box furnaces. If the reactants are volatile and vulnerable to the oxygen in air, experiments are supposed to be performed in a sealed tube with or without certain gas flowing over the reactant during heating and cooling processes.

The solid state synthesis route consists of two steps of thermal treatments, calcination and sintering, which take place below the melting temperatures of the materials. The function of calcination is to remove undesired substances by decomposition and volatilization and to homogenize the material and to alleviate material shrinkage for the subsequent sintering process. Sintering is a technique based on atomic diffusion at higher temperature. Thermal expansion caused by the diffusion of atoms diminishes the area between two grains in contact. Atoms in solids are compressed on the surface of their neighboring grains by diffusion of atoms across the boundaries of grains, which increase the density of ceramics.

2.5 synthesis routes for nanoscale $BiFeO_3$

Many techniques have been utilized to prepare $BiFeO_3$ nanostructures. The thin films $BiFeO_3$ always exhibit stronger remnant polarization than bulk $BiFeO_3$, which was reported to be attributed to the strain enhancement and to the existence of the impurity phase of τ–Fe_2O_3 in the thin film of $BiFeO_3$.[21]

Thin $BiFeO_3$ films can be fabricated by techniques like PLD (Pulsed Laser Depostion). A target of $BiFeO_3$ in condensed pellet form is first placed in a vacuum chamber and then struck by a focused pulsed laser beam in vacum. The samples evaporates under laser striking and the thin film of $BiFeO_3$ is subsequently deposited on a substrate/wafer made from Si,[22] $SrTiO_3$[23] or $DyScO_3$[24]. Wet chemical methods are always chosen to fabricate $BiFeO_3$ nanoparticles. Appropriate techniques are selected depending on the criteria emphasized, such as particle size and distribution, temperaturen, etc.. Sol-gel method is one of the popular synthesis techniques which can synthesize metal oxide by steps of hydrolysis and condensation of precursors (usually metal alkoxides or metal oxides). The gel obtained is in a solid phase after steps of aging, drying and densification steps. The size of the fabricated nanoparticles is between 15-150 nm depending on the process of hydrolysis and drying. The sol-gel method of obtaining uniform porous powders can be mass produced and applied to the industry.[25]

3. Experimental results on $BiFeO_3$ and related compounds

3.1 $xBiFeO_3$-(1-x) $SrTiO_3$

$BiFeO_3$ (rhomobohedral R3c, $a^-a^-a^-$ in Glazer notation) is one of the few multiferroics exhibiting ferroelectricity and antiferromagneticity simultaneously. Extremely weak ferromagnetism is also detected in the bismuth ferrite due to its unique spin-canting structure. This spin-canted antiferromagnetism is a result of the deflection of antiparallel magnetic moments from the antiferromagnetic plane, which gives rise to a weak net magnetism.[26]

$SrTiO_3$ is a typical stable paraelectric perovskite at room temperature which is centrosymmetric (cubic Pm-3m with $a^0a^0a^0$ in the Glazer notation). By introducing $SrTiO_3$ to the $BiFeO_3$ system, the drawback of low electrical resistivity and instability of $BiFeO_3$ can be avoided,[27, 28] providing desired stabilization and high electric resistivity suitable for dielectric (ferroelectric) measurements and industry application.

Experimental

Powdered polycrystalline sample of $xBiFeO_3$-(1-x)$SrTiO_3$ (x=0.1-0.7) were fabricated by solid state reaction method. The starting materials were bismuth oxide Bi_2O_3 (Sigma-Aldrich, 99.99%), iron oxide Fe_2O_3 (Alfa Aesar, 99.998%), strontium carbonate $SrCO_3$(Aldrich, >99.9%) and titanium dioxide TiO_2 (Aldrich, >99%). Appropriate molar ratio of the above powders were mixed and ground in an agate mortar for about 30 minutes, a small amount of ethanol served as a milling aid sprayed on the mixed power. The mixed powders were transferred to the alumina crucibles, placed in an oven and calcined at 700°C for 12 hours with heating rate of 5°C/min. Then, the calcined powders were milled again and pressed into pellets with a diameter of 10mm. Subsequently, the powders were sintered at 800°C or 900°C for 20 hours, followed by a repeated procedure of milling, pelletizing and sintering at temperatures ranging from 900°C to 1150°C. The cycle was repeated once again for the compositions of x=0.6, 0.7 at 965°C and 0.1 at 1200°C. Table 3.1 reveals the temperatures and durations during the thermal treatments.

Solid solution	Thermal treatment			
$xBiFeO_3$-(1-x) $SrTiO_3$	Calcination (12h)	Sintering 1(20h)	Sintering 2(20h)	Sintering 3(12h)

x=0.1	700°C	900°C	1150°C	1200°C
x=0.2	700°C	900°C	1100°C	-
x=0.3	700°C	900°C	1100°C	-
x=0.4	700°C	900°C	1000°C	-
x=0.5	700°C	800°C	1000°C	-
x=0.6	700°C	800°C	900°C	965°C
x=0.7	700°C	800°C	900°C	965°C

Table 3.1 Calcinations and sintering temperatures for solid solution of $xBiFeO_3$-(1-x) $SrTiO_3$.

X-Ray diffraction result

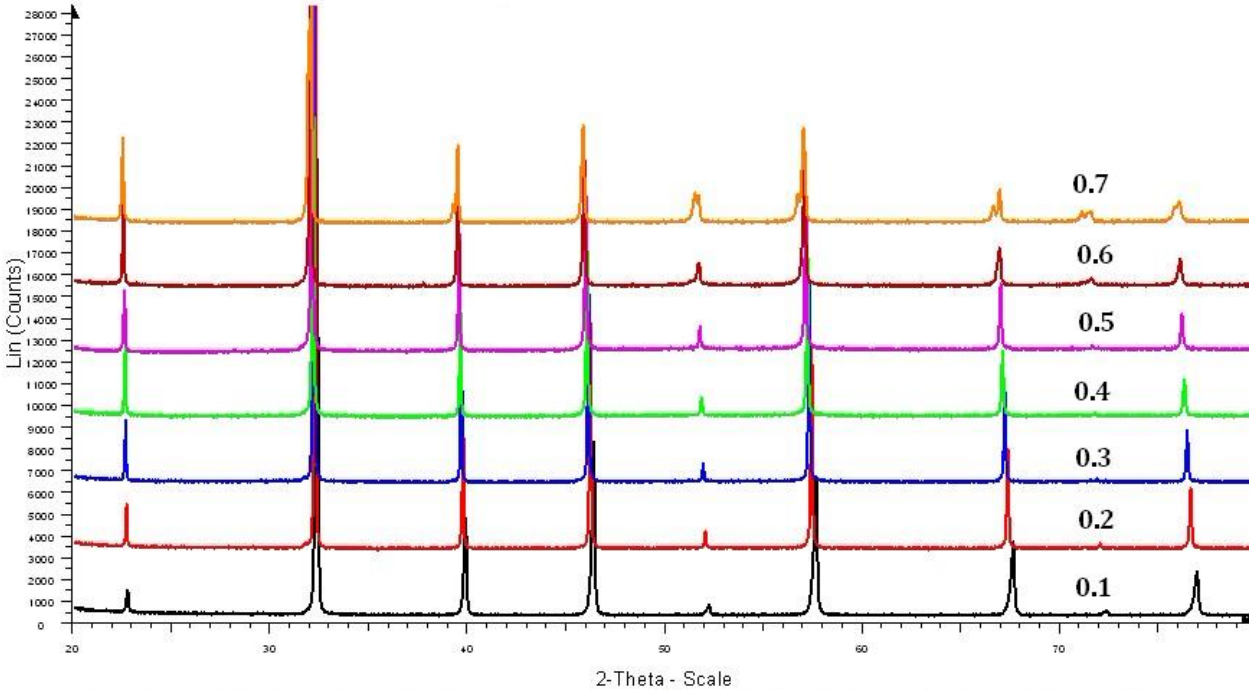

Figure 3.1 Powder x-ray diffractograms for $xBiFeO_3$-(1-x) $SrTiO_3$ (x=0, 0.1, 0.2, 0.3, 0.4, 0.5, 0.6 and 0.7).

The solid solution series of $xBiFeO_3$-(1-x)$SrTiO_3$ was characterized by the powder x-ray diffraction technique. Cubic perovskite structure with almost no impurity phase was observed up to 0.6, as illustrated in Figure 3.1. However, it is worth noting that peaks at 2θ=52°, 67° and 72° are split when x reaches 0.7. It can be explained as an occurrence of a structural phase transition to the rhombohedral structure of $BiFeO_3$. It is expected that an inclination to the rhombohedrally distorted R3c structure would be obtained if the content of bismuth ferrite in the system was raised further.

Since the structures of solid solutions $xBiFeO_3$-(1-x) $SrTiO_3$ (x=0.1-0.6) are cubic Pm-3m, lattice parameter within this range was calculated by program Celref, as shown in Figure 3.2.

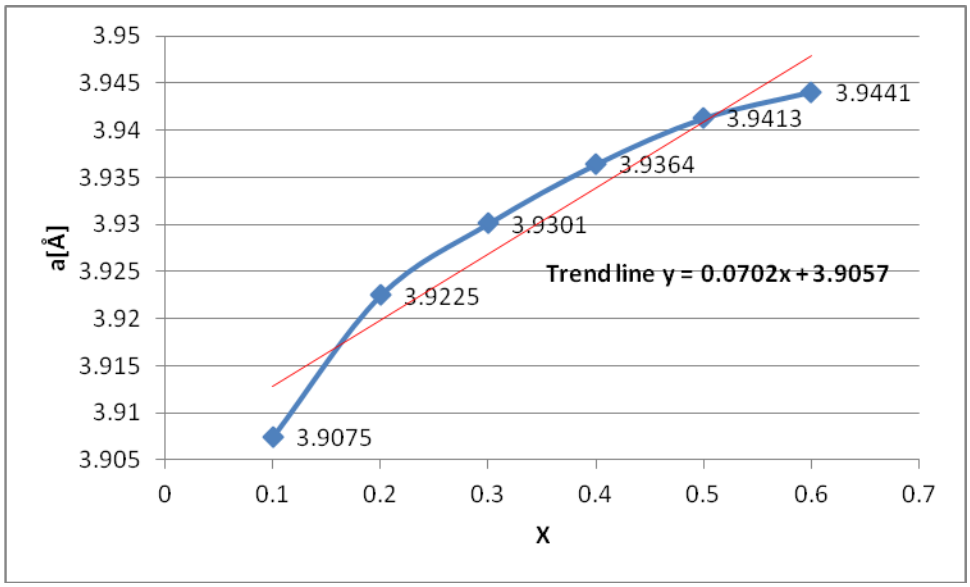

Figure 3.2 Fitted lattice parameter for the solid solution of $xBiFeO_3$-(1-x) $SrTiO_3$

The lattice parameter is proportional to the composition of bismuth ferrite in the solid solution. Although the sum of ionic radii of Bi^{3+} (1.17 Å, 8-coordinate) and Fe^{3+} (0.645 Å, 6-coordinate, high spin) are less than the sum of ionic radii of Sr^{2+} (1.18 Å, 6-coordinate) and Ti^{4+} (0.605 Å, 6-coordinate), the two outer 6s electrons (lone pairs) in Bi^{3+} are quite active that makes the lone pairs ordered in one direction to hybridize with oxygen 2p orbital, resulting in a bigger ionic radii of Bi^{3+} than the value obtained from the database. The ionic radii of Bi^{3+} plays a dominant role in the overall cell parameter of the binary solution, the cell parameter is increased by substitution of $BiFeO_3$ for the $SrTiO_3$.

Magnetic properties

Figure 3.3 shows the M-H (external magnetic field versus magnetization) curves of binary solid solution of $xBiFeO_3$-(1-x) $SrTiO_3$ (x=0.1-0.7) measured at 5K.

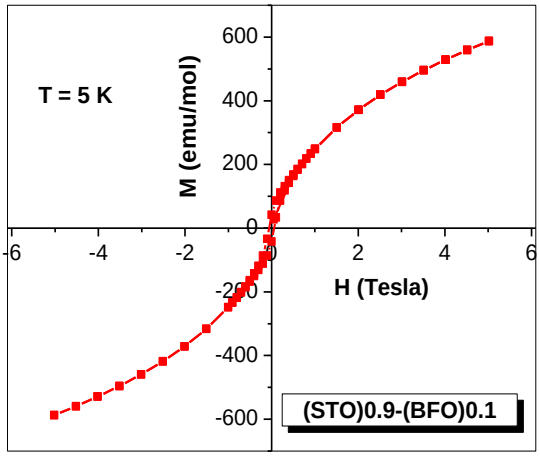
T = 5 K
M (emu/mol)
H (Tesla)
(STO)0.9-(BFO)0.1

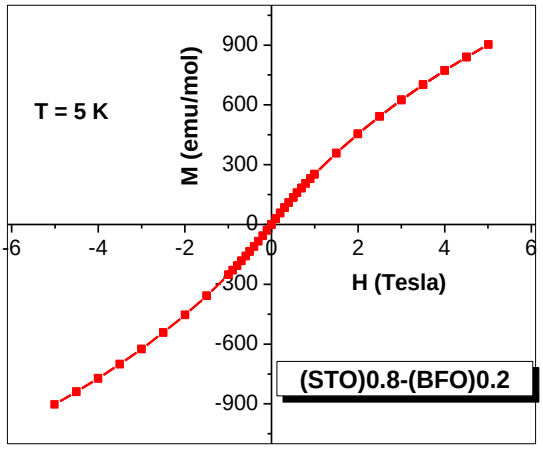
T = 5 K
M (emu/mol)
H (Tesla)
(STO)0.8-(BFO)0.2

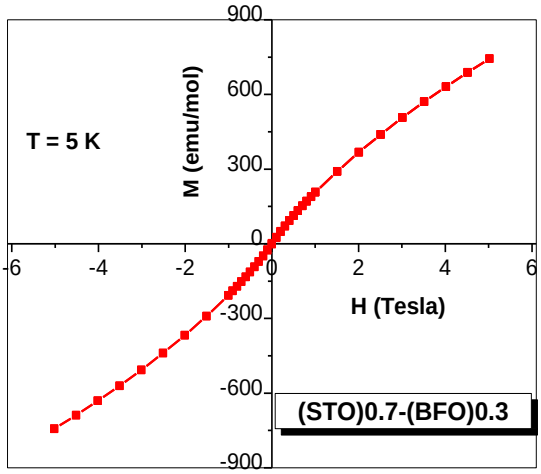
T = 5 K
M (emu/mol)
H (Tesla)
(STO)0.7-(BFO)0.3

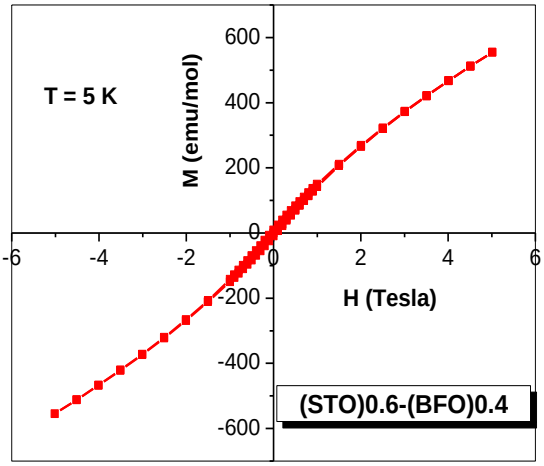
T = 5 K
M (emu/mol)
H (Tesla)
(STO)0.6-(BFO)0.4

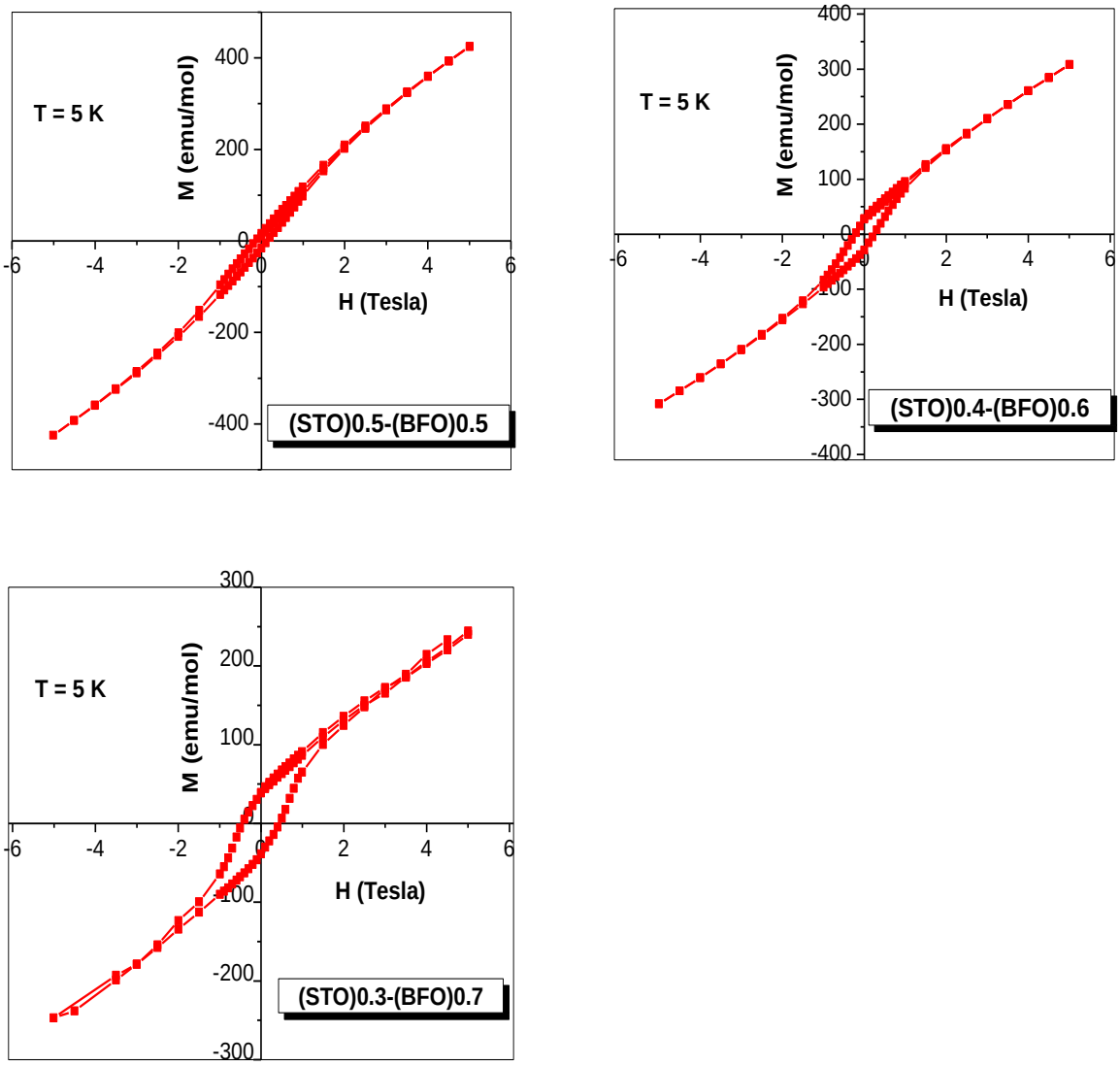

Figure 3.3 M-H loops of $xBiFeO_3$-(1-x) $SrTiO_3$ (x=0.1-0.7) at 5K.

As can be seen, nearly no hysteresis loops are found for x=0.1, 0.2 and 0.3. In particular, for x=0.1 it is basically paramagnetic characterized by the nonlinear magnetization with slope greater than 1 at low magnetic field and no remnant magnetization being detected. The paramagnetism becomes weaker as the composition of bismuth ferrite increases, where remnant magnetization becomes obviouse at x>0.4. The $0.7BiFeO_3$-$0.3SrTiO_3$ shows the largest values for magnetization of nearly 45emu/mol with coercive field of 5 Tesla. This magnetization behaviour of solid solution $xBiFeO_3$-(1-x) $SrTiO_3$ is quite consistent with that of the $xBaTiO_3$-(1-x) $BiFeO_3$ system published by J. S. Kim et al.[30] and A. Y. Kim[31]. For our target samples, as more bismuth ferrite incorporated in the system, they become antiferromagnetic with weak ferromagnetism in the compositional range of x=0.4-0.7. The presence of the remnant magnetization is attributed to the

uncompensated antiferromagnetic spin in the solid solution. At x=0.7, it is characterized by the rhombohedral structure which has the largest ferromagnetic component.

3.2 Isovalently substituted multiferroic $BiFeO_3$

3.2.1 $Bi_{1-x}La_x FeO_3$

In an attempt to acquire stronger magnetoelectrical coupling and to alleviate the impurities produced during the synthesis, isovalent substitution on the A-site bismuth is considered, and traces of rare-earth element lanthanum is chosen to replace A-site bismuth.

Since the bismuth ferrite possesses antiferromagnetic order along $[001]_h$ direction, this canted antiferromagnetic sublattices have weak magnetization. In the meanwhile, a sinusoidal spin structure along $[110]_h$ direction cancels out this macroscopic magnetization, which leads to a strong restriction on the magnetoelectric effect. Rare-earth substituted bismuth ferrite can enhance the magnetism of $BiFeO_3$ by suppressing the spin-cycloid structure and improve the ferroelectricity by increasing the compositional stability.[32, 33 34, 35]

Different substituted elements have different ionic sizes and concentrations, which changes the original symmetry of $BiFeO_3$. For example, the A-site bismuth is replaced by a trace amount of lanthanum, by coincidence, the ionic sizes of La^{3+} (116pm, 8-coordinate) and Bi^{3+} (117pm, 8-coordinate) are quite adjacent, this substitution can dilute the concentration of Bi^{3+} in the system and influence the ferroelectric effect caused by the lone pair electrons.

Experimental

Conventional solid state synthesis route to prepare nanoparticles is a time-consuming and energy-consuming work that requires high temperature over a long period of time. Chemical reaction happens at that temperature by breaking chemical bonds first, followed by the immigration of ions within the solid. Undesired impurities might be obtained if powders are not well mille or unexpected volatilization. Because of the volatility of the bismuth ions and instability of bismuth ferrite at high temperature, the formation of impurity phases like $Bi_{25}FeO_{39}$ and Bi_2FeO_9 together with ferrous ion compounds and oxygen vacancies are possible, which could affect the measurement of dielectric or ferroelectric properties.

To overcome this problem, many synthesis routes have been investigated, like hydrothermal, sol-gel, combustion, microemulsion and coprecipitation routes. In this thesis work, coprecipitation route was chosen to synthesize bismuth ferrite, and polycrystalline powders with high purity and crystallinity were obtained. However, the particle size distribution was quite broad due to the difficulty of controlling the fast precipitation speed. Recently, modification to the coprecipitation route has been reported by keeping the alkalinity of solution constant though adding nitrate and ammonia solution.[36]

For $Bi_{1-x}La_xFeO_3$ (x=0, 0.1, 0.15, 0.175, 0.2), stoichiometric amounts of $Bi(NO_3)_3{\cdot}4.86H_2O$, $Fe(NO_3)_3{\cdot}8.28H_2O$ and $La(NO_3)_3{\cdot}5.26H_2O$ were weighed beforehand (the hydration of water in the nitrates sample were initially calculated from TGA experiments, as shown in Figure 3.4). Then 6.5ml 69 % of concentrated nitric acid and 43.5 ml deionized water were mixed in a small beaker. Subsequently, nitrates of iron, bismuth and lanthanum were added into the beaker with magnetic stirring at 80°C on a hot plate. A homogeneous precursor solution was obtained after continuous stirring for 30 minutes, and the solution was transferred into an acid burette. In parallel, another beaker with the mixture of 30ml of 25% ammonia and 300ml deionized water was prepared. Subsequently, the precursor solution was gradually dripped into the ammonia solution under strong magnetic stirring. In the meantime, a pH meter was used to measure the pH of the ammonia solution. The pH was adjusted to be close to 9 by compensating with extra ammonia solution if necessary. Once the whole acid solution in the acid burette was consumed, the precipitate was filtered and washed with ethanol twice. Dark powders were obtained after the thermal treatment in the oven at 180°C for overnight. Finally, powders were ground and sintered at different temperatures (500°C-800 °C) for 2 hours. Powder x-ray diffraction technique was applied to characterize the specimens after each thermal treatment.

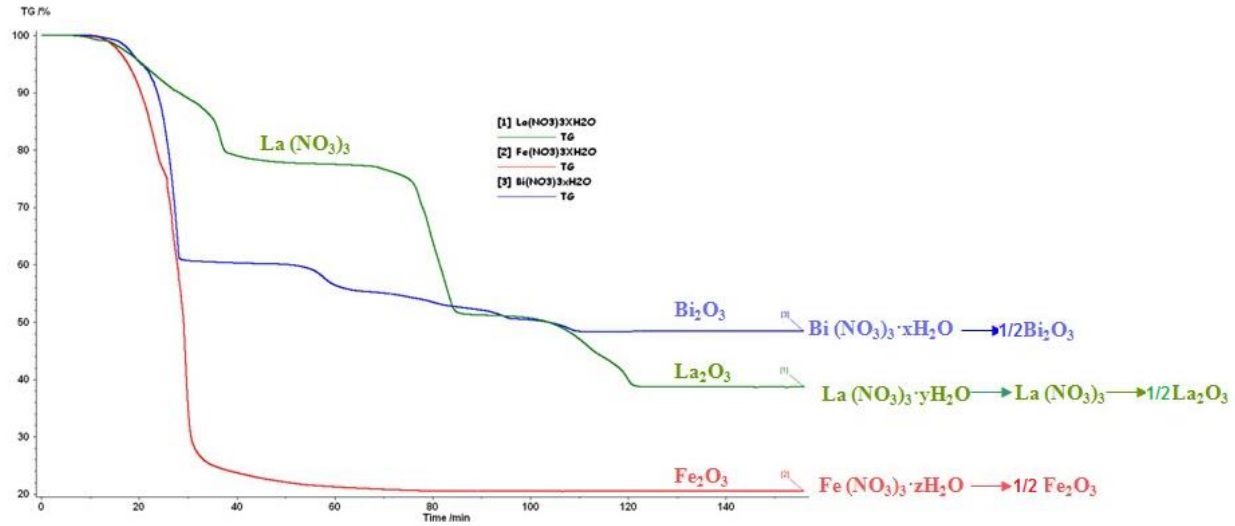

Figure 3.4 Determination of the amount of hydration in the nitrate compounds by TGA.

X-Ray diffraction result

Polycrystalline structures of $Bi_{0.85}La_{0.15}FeO_3$ was synthesized and characterized by Bruker D8 advance diffractometer with Cu $K\alpha_1$. It has been reported that the influence of pressure and temperature on the polycrystalline structure are quite significant. Convincing example is illustrated in Figure 3.5, the $Bi_{0.85}La_{0.15}FeO_3$ was first sintered at 700°C for 2 hours and then at 800°C for another 2 hours, subsequently, the powdered compound was pressed into a 13mm pellet with thickness of only 1 mm at 7 tons pressure. It is worth noting that the peaks become more sharp at 800°C indicating an increased in crystallinity of the test compound. When the powder was subjected to an extra pressure of 7 tons, peak at $2\theta=39°$ diminishes while a tiny peak burgeons at $2\theta=46.5°$ reflecting the occurrence of phase transformation from R3c into Pbam. The effect of pressure is comparable to the internal stresses within ceramics, which initiates a route from the polar to the nonpolar symmetries.[37]

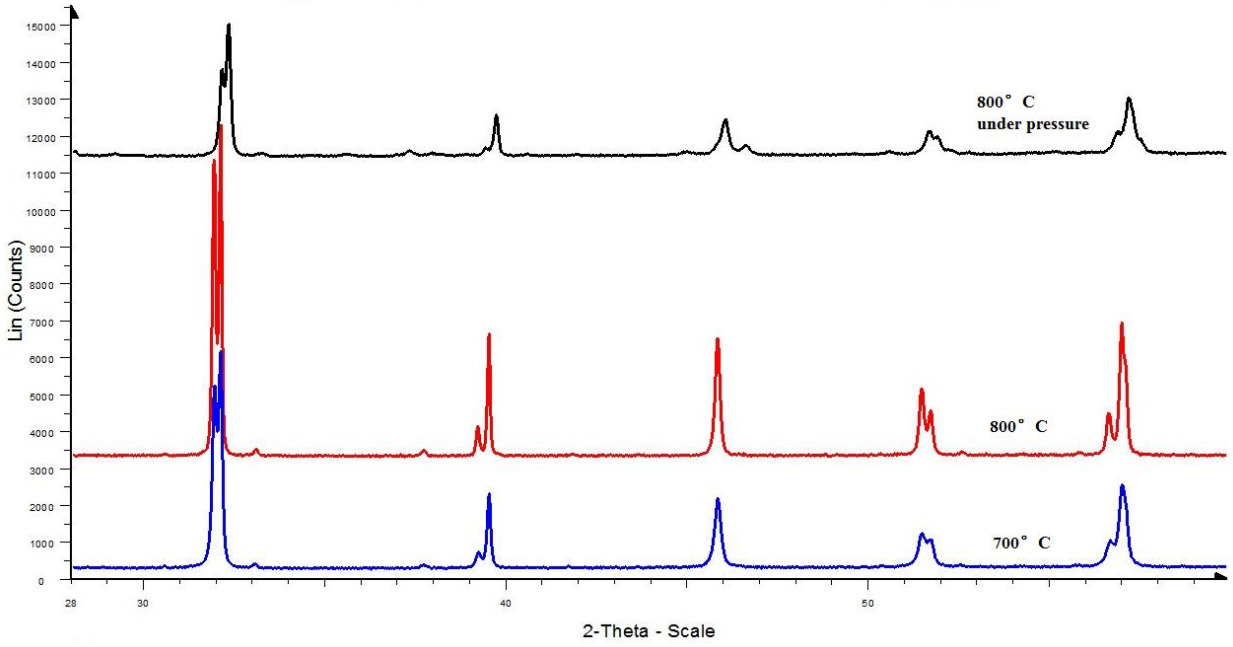

Figure 3.5 Comparison of x-ray diffraction patterns for the $Bi_{0.85}La_{0.15}FeO_3$ at different temperatures and pressures.

The long scan diffraction patterns of polycrystalline structures of the $Bi_{1-x}La_xFeO_3$ series after heating at 800°C are presented below in Figure 3.6.

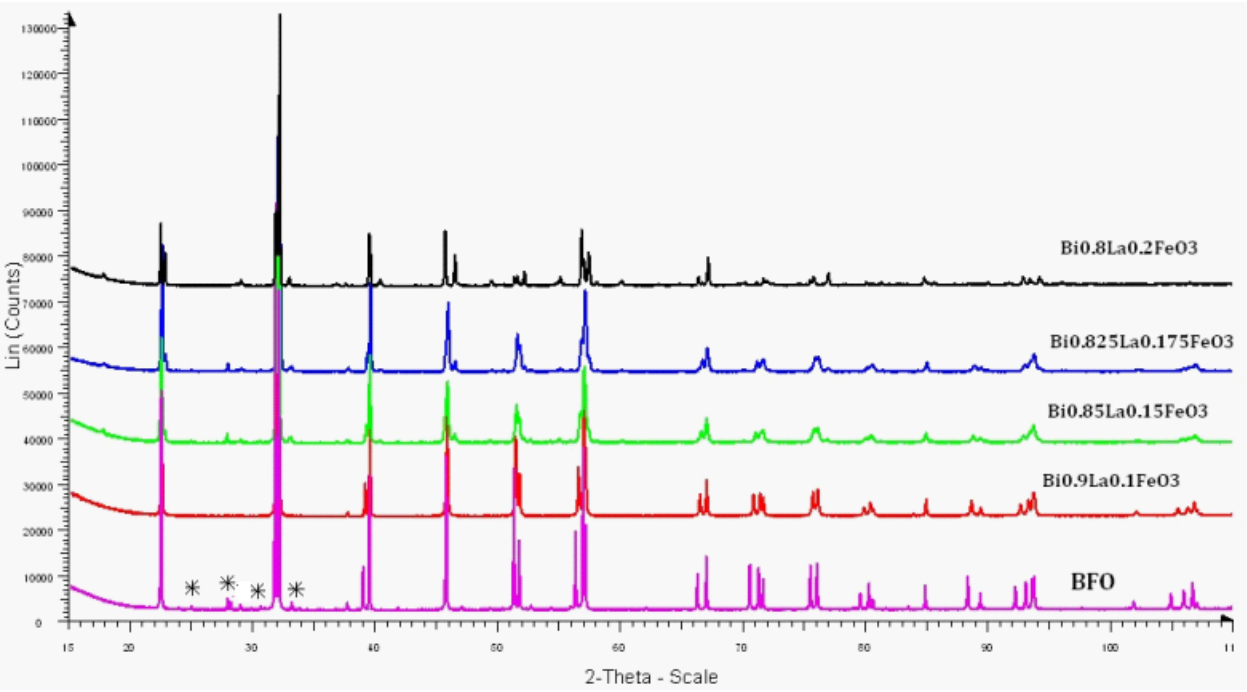

Figure 3.6 Stack plot of long scan X-Ray diffraction patterns for the $Bi_{1-x}La_xFeO_3$ series after heating at 800°C (x=0, 0.1, 0.125, 0.15, 0.2). *Impurity phase $Bi_{25}FeO_{39}$ is illustrated for the BFO (bismuth ferrite) sample.

According to the Figure 3.6, as lanthanum content increases in the series, a new structure characterized by $PbZrO_3$-type Pbam appears, which constitutes 19.60 wt% at x=0.15 from Rietveld analysis appears as shown in Table 3.4. The intensities of some diffraction peaks, e.g. a small peak at 2θ≈46.5° starts to grow, while the peak at 2θ≈39° tends to disappear. When x=0.175, a two-phase region is clearly seen where the Pbam phase is composed of 29% of the total weight (see Table 3.5). It is apparent that the phase transformation from R3c is complete at x=0.2, the diffraction peaks are characterized by the single phase orthorhombic structure of $PbZrO_3$-type Pbam.

Rusakov et al. also investigated the $Bi_{1-x}La_xFeO_3$ (x>0.2), they reported that the La substituted bismuth ferrite keeps in a single phase characterized by $PbZrO_3$-type Pbam which cannot be changed until x=0.3. [37] The $GdFeO_3$-type Pnma ($a^+b^-b^-$ by Glazer notation) structure can formed above x=0.5.[37]

Rietveld Refinement

Rietveld refinements were performed in order to get detailed structural parameters of the $Bi_{1-x}La_xFeO_3$ series. As discussed above, R3c and Pbam models were utilized to model the rhombohedral and orthorhombic components within the two phase region of x=0.15 and x=0.175, while R3c model was only adopted for x=0 and 0.1. Structural information after Rietveld refinements were summarized below.

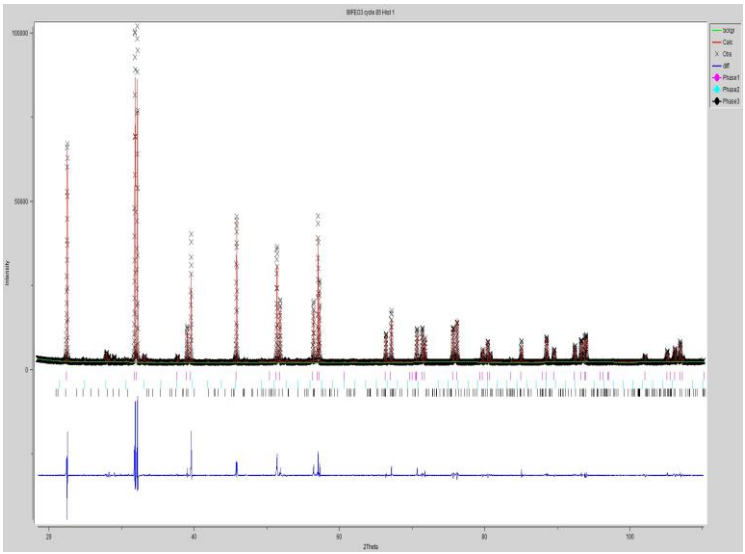

Figure 3.7 Rietveld analysis of the powder diffraction data from $BiFeO_3$. Crosses represent observed data points, the red line is the calculated diffraction data while the blue line indicates the difference between the observed and calculated intensities. Tick marks show the peak positions of R3c (pink color), impurity phase Bi_2FeO_9 (cyan color) and $Bi_{25}FeO_{39}$ (black color) structures.

Crystal Structure parameters of the $BiFeO_3$

Rhombohedral structure with R3c space group, wt. Frac.:91.66%
Atomic position
Bi(0, 0, 0.041584); Fe(0, 0, 0.263104); O(0.433205, 0.017745, 0)
Crystal axes (Å) and crystal axial angle (°)
α= 90; β= 90; γ=120; a=5.577352; b=5.577352; c=13.867785
Volume(Å^3)
373.529
R value of Rietveld refinements
R_{wp}= 8.14%; R_p=4.67%; χ^2=19.61

Table 3.2 Refined structural parameters for $BiFeO_3$ determined by Rietveld analysis.

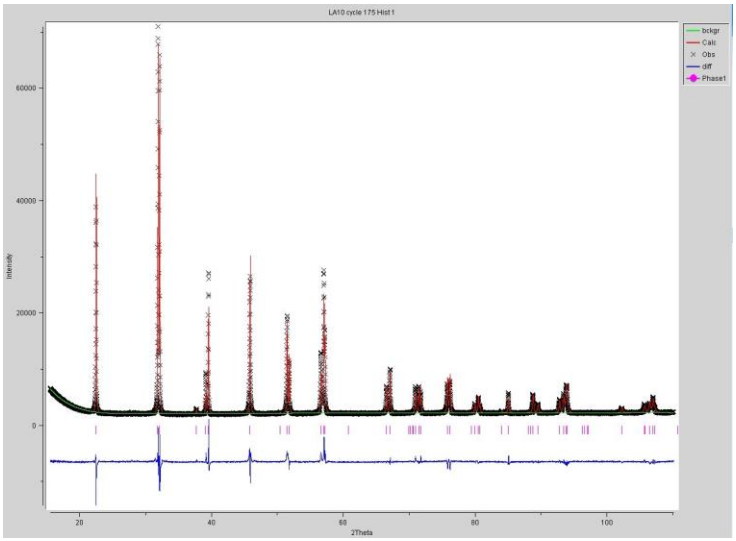

Figure 3.8 Rietveld analysis of the powder diffraction data from $Bi_{0.9}La_{0.1}FeO_3$. Tick marks show the peak position of R3c structure $Bi_{0.9}La_{0.1}FeO_3$.

Crystal Structure parameters of the $Bi_{0.9}La_{0.1}FeO_3$

Rhombohedral structure with R3c space group
Atomic position
Bi(0, 0, 0); La(0, 0, 0); Fe(0, 0, 0.223967); O(0.435454, -0.015260, 0.959105)
Crystal axes (Å) and crystal axial angle (°)
α= 90; β= 90; γ=120; a=5.576058; b=5.576058; c=13.807185
Volume(Å^3)
371.784
R value of Rietveld refinements
R_{wp}= 5.97%; R_p=3.91%; χ^2=10.17

Table 3.3 Refined structural parameters for $Bi_{0.9}La_{0.1}FeO_3$ determined by Rietveld analysis.

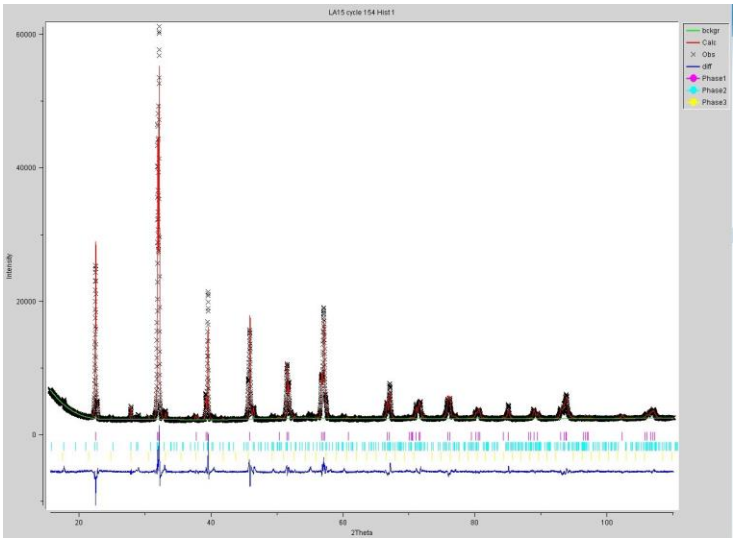

Figure 3.9 Rietveld analysis of the powder diffraction data from $Bi_{0.85}La_{0.15}FeO_3$. Tick marks show the peak positions of R3c (pink color), Pbam(cyan color) and impurity $Bi_{25}FeO_{39}$ (yellow color) structures.

Crystal Structure parameters of the $Bi_{0.85}La_{0.15}FeO_3$

Rhombohedral structure with R3c space group, wt. Frac.:78.15%

Atomic position

Bi(0,0,0); La(0,0,0); Fe(0,0,0.227596); O(0.452,0.0183,0.9624)

Crystal axes (Å) and crystal axial angle (°)

α= 90; β= 90; γ=120; a=5.577687; b=5.577687; c=13.773235

Volume($Å^3$)

371.086

Orthorhombic structure with Pbam space group wt. Frac.:19.60%

Atomic position

Bi-1(0.735,0.1367,0);La1(0.735,0.1367,0); Bi-2(0.742,0.1186,0.5); La-2(0.742,0.1186,0.5);
Fe(0.232,0.1243,0.2459); O-1(0.259,0.169,0); O-2(0.273,0.077,0.5); O-3(0.008,0.242,0.291);
O-4(0,0.5,0.203); O-5(0,0,0.205)

Crystal axes (Å) and crystal axial angle (°)

α= 90; β= 90; γ=90; a=5.625411 b=11.214787; c=7.823177

Volume($Å^3$)

493.547

R value of Rietveld refinements

R_{wp}= 5.51%; R_p=3.76%; χ^2=9.323

* impurity phase $Bi_{25}FeO_{39}$

Table 3.4 Refined structural parameters for $Bi_{0.85}La_{0.15}FeO_3$ determined by Rietveld analysis.

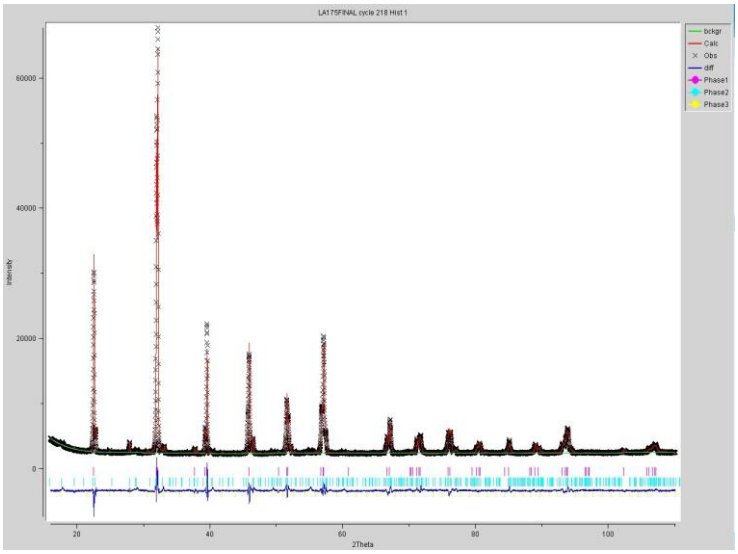

Figure 3.10 Rietveld analysis of the powder diffraction data from $Bi_{0.825}La_{0.175}FeO_3$.

Crystal Structure parameters of the $Bi_{0.825}La_{0.175}FeO_3$

Rhombohedral structure with R3c space group, wt. Frac.:68.71%

Atomic position

Bi(0,0,0); La(0,0,0); Fe(0,0,0.227598); O(0.452,0.0183,0.9624)

Crystal axes (Å) and crystal axial angle (°)

α= 90; β= 90; γ=120; a=5.578439; b=5.578439; c=13.764944

Volume($Å^3$)

370.963

Orthorhombic structure with Pbam space group wt. Frac.:29.00%

Atomic position

Bi-1(0.735,0.1367,0);La1(0.735,0.1367,0); Bi-2(0.742,0.1186,0.5); La-2(0.742,0.1186,0.5);

Fe(0.232,0.1243,0.2459); O-1(0.259,0.169,0); O-2(0.273,0.077,0.5); O-3(0.008,0.242,0.291);

O-4(0,0.5,0.203); O-5(0,0,0.205)

Crystal axes (Å) and crystal axial angle (°)

α= 90; β= 90; γ=90; a=5.613879; b=11.189156; c=7.805886

Volume($Å^3$)

490.323

R value of Rietveld refinements
R_{wp}= 4.59%; R_p=3.31%; χ^2=6.466
* Impurity phase $Bi_{25}FeO_{39}$

Table 3.5 Refined structural parameters for $Bi_{0.825}La_{0.175}FeO_3$ determined by Rietveld analysis

Rietveld analysis of diffraction patterns are used to identify the derivation of all the diffraction peaks and to distinguish different structures from peaks as well as measure different structural compositions quantitatively. Refinement work on the $Bi_{1-x}La_xFeO_3$ (x=0.1, 0.15, 0.175) series reveals a superposition of two structures, R3c and Pbam, coexist in the material for the composition of x=0.15 and 0.175. According to the tables above, for the diffraction pattern of x=0.15, approximately 78.15% of the contribution was made by a rhomobohedral R3c structure while another 19.60% is made up of antipolar orthorhombic structure of $PbZrO_3$-type Pbam. With the content of lanthanum increases in the series, the compound $Bi_{0.825}La_{0.175}FeO_3$ is composed of 68.71% R3c and 29.00% Pbam, which indicates an increase in the amount of orthorhombic structure. In addition, it is worth mentioning that slight traces of $Bi_{25}FeO_{39}$ impurity is always accompanied by the formation of $BiFeO_3$-related compound. However, for the $Bi_{0.9}La_{0.1}FeO_3$, it is identified as having only one phase characterized by a rhomobohedrally distorted R3c structure.

To conclude, by replacing bismuth with traces of lanthanum, the stereochemically active lone pair Bi, which accounts for the rohombohedral polar structure, is gradually diluted and diminished. The lanthanum substituted bismuth ferrite implies a composition-driven transition in a sequence of R3c to Pbam.

The conclusion is in accordance with previous structural investigation of $Bi_{1-x}Ln_xFeO_3$ (Ln=La, Nd, Sm, Gd) series,[39, 40] which reveals that the $PbZrO_3$-type orthorhombic structure is stabilized within a concentration range between rhomobohedrally distorted R3c and nonpolar orthorhombic Pnma.

Thermal analysis

To determine the antiferromagnetic (T_{Neel}) and ferroelectric (T_{Curie}) ordering temperature of $Bi_{1-x}La_xFeO_3$ ($0 \leq x \leq 0.2$) , differential thermal analysis have been performed on this compound series.

Differential scanning calorimetric measurements of $Bi_{1-x}La_xFeO_3$ (x=0.1, 0.15, 0.175 and 0.2) series were performed at temperature between 150°C and 850°C under argon flow. Sample was placed in a small Platinum crucible and underwent a heating and a cooling process at rate of 10K/min. The data obtained are displayed below in Figure 3.11 and 3.12.

According to the two DSC graphs, the peaks from exothermic process appears approximate 20°C lower than

those peaks located in endothermic process, which means that more peaks can be seen in the cooling process. Thus, in this thesis, the peaks presented in the exothermic process were analyzed.

The curves in the figures below can be primarily classified into three categories depending on different amount of lanthanum in the compound. x=0.15 and 0.175 is the first group which have three distinct peaks that correspond to the Neel temperature point, phase transformation from mixed phase region of R3c and Pbam to Pnma, and transition from Pnma to cubic. However, for the second group x=0 and x=0.1, the structure at low temperature region is only characterized by the single phase R3c, therefore, the two peaks from this group refer to the Neel temperature and ferroelectric transition from antipolar R3c to nonpolar Pnma. On the contrary, for x=0.2 there is no R3c structure but only Pbam structure exhibited at low temperature, the two peaks, from left to right, serves as the Neel point and transformation from Pbam to Pnma (without Curie point) respectively.

Neel and Curie temperature were summarized in the Table 3.6, it is noted that the Neel temperatures are less sensitive to the compositional change while the Curie temperature decrease rapidly with the increase of lanthanum in system, which are comparable to the temperature reported in literatures.

$Bi_{1-x}La_xFeO_3$		
x	T(Neel)/°C	T(Curie)/°C
0	363	814
0.1	380	668
0.15	383	560
0.175	385	516
0.2	385	

Table 3.6 Curie and Neel temperature of $Bi_{1-x}La_xFeO_3$ summarized from cooling process.

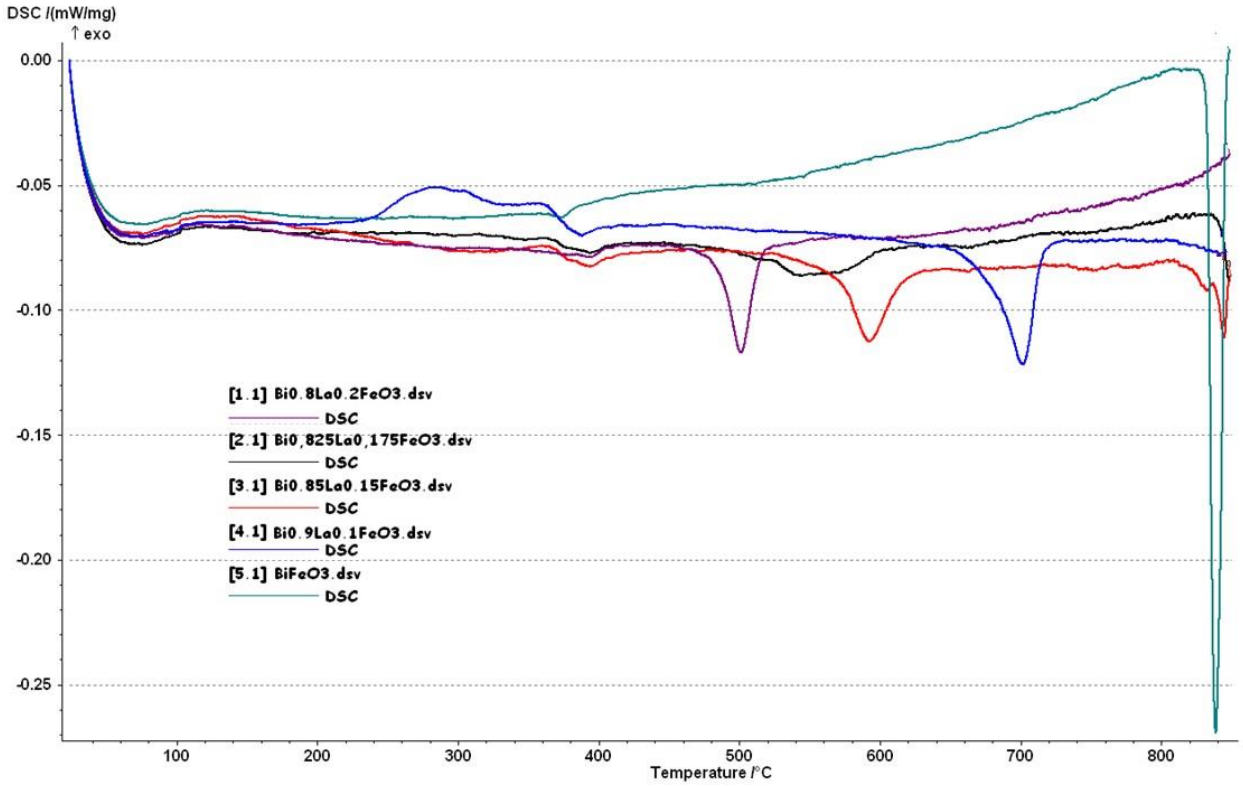

Figure 3.11 DSC plot of $Bi_{1-x}La_xFeO_3$ ($0 \leq x \leq 0.2$) during the heating process.

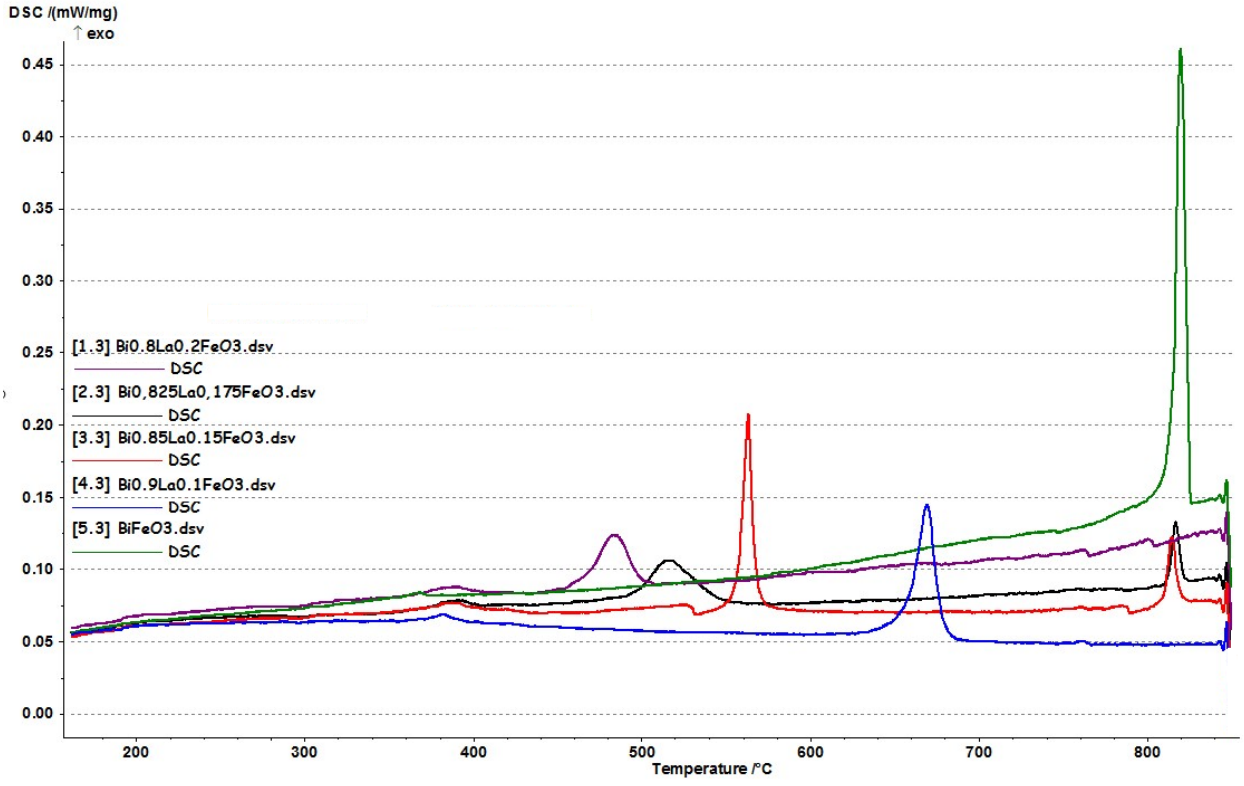

Figure 3.12 DSC plot of $Bi_{1-x}La_xFeO_3$ ($0 \leq x \leq 0.2$) during the cooling process.

3.2.2 $Bi_{1-x}Tb_xFeO_3$

Experimental

The coprecipitation route was chosen to synthesize Tb doped bismuth ferrite $Bi_{1-x}Tb_xFeO_3$ (x=0.05, 0.1, 0.125, 0.15, 0.175 and 0.2). Apart from using terbium nitrate rather than lanthanum nitrate, the experiment procedure is exactly the same as making La doped bismuth ferrite.

X-Ray diffraction result

Powder state polycrystalline $Bi_{1-x}Tb_xFeO_3$ series (x=0.05, 0.1, 0.125, 0.15, 0.175 and 0.2) were examined by the same x-ray diffraction technique used for determination of La bismuth ferrite (λ=1.54056Å, 28-60° 2θ, 0.021° step size, 28minutes). With respect to the Tb doped $BiFeO_3$, more patterns with different Tb contents than that of the La are shown below in Figure 3.13 after final heating at 800 °C.

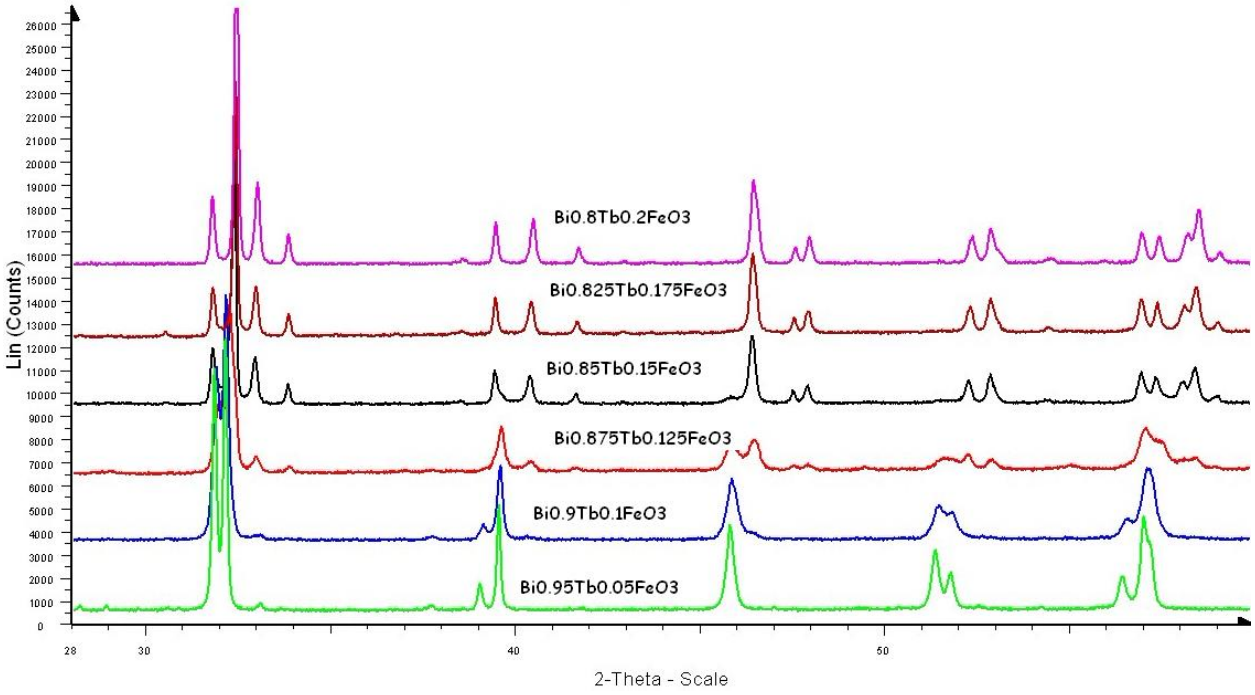

Figure 3.13 Stack plot of long scan X-Ray diffraction patterns showing the effect of increasing $Bi_{1-x}Tb_xFeO_3$ series ($0.05 \leq x \leq 0.2$).

By looking at the Figure 3.13, rhombohedrally distorted perovskite structure R3c is still retained at x=0.05, with existence of small amount of $Bi_{25}FeO_{39}$ impurity. As the content of terbium increases, a two-phase region is obtained in the interval of x=0.1-0.15 with both rhombohedral R3c and orthorhombic Pnma. However, from x=0.175 and 0.2, it is obvious that the phase transition is terminated with single phase orthorhombic Pnma demonstrated.

In comparison with lanthanum, the $PbZrO_3$-type Pbam structure is unstable that can not be seen in the phase transformation of the terbium substituted bismuth ferrite, whereas the R3c ->Pbam ->Pnma sequence of the substitution-induced transition is only observed for the $Bi_{1-x}La_xFeO_3$. Such difference derives from their ionic sizes, since the ionic radius of La^{3+} (116pm, 8-coordinate) is comparable to the that of the original Bi^{3+} (117pm, 8-coordinate) while the radius for Tb^{3+} is rather small (104pm, 8-coordinate). The large difference in ionic radii impedes the formation of antipolar orthorhombic structure which is less stable in that condition.

In addition, apart from the chemical substitution-induced phase transition, the sintering temperature as well as pressure also influence or change polycrystalline structures.[41] I.O. Troyanchuk et al. reported a pressure-induced phase transformation from R3c to Pbam of the solid-state synthesized $Bi_{0.82}La_{0.18}FeO_3$ powder at a much higher pressure.[42] Because of the large difference between the ionic radii between original and substituted elements, the changed interatomic distance by chemical substitution is comparable to the external pressure applied to the polycrystalline powders which acts as the internal stresses inside materials.[43, 44]

In recent years, except for the isovalent substitution on the A-site, there has been a growing interest focusing on the isovalent substitution on the B-site in perovskite compounds, which might lead to other structural changes and stronger magnetoelectrical couplings. Neutron diffraction shows a phase transition towards space group Imma ($a^0b^-b^-$) started at x=0.15 for the investigation of B-site substituted $Bi_{0.9}Sm_{0.1}Fe_{1-x}Mn_xO_3$ system. This transition accords with the loss of an antiphase tilts R3c ($a^-a^-a^-$) and the Imma ($a^0b^-b^-$) serves as intermediate between original R3c and $GdFeO_3$-type Pnma ($a^+b^-b^-$), which we observed here for $Bi_{0.8}Tb_{0.2}FeO_3$.[45]

Conclusion

To conclude, the diffraction results of binary solid solution $xBiFeO_3$-$(1-x)SrTiO_3$ demonstrate a transformation from the nonpolar cubic structure to the antipolar rhombohedral structure on the edge of x=0.7. In the meantime, magnetic measurement reveals the paramagnetism in $xBiFeO_3$-$(1-x)SrTiO_3$ ceramics at low x progressively transforms into antiferromagnetism with relatively weak ferromagnetism due to the influence of the uncompensated antiferromagnetic spin in the ceramics.

Study on the $Bi_{1-x}La_xFeO_3$ ($0\leq x\leq 0.2$) and $Bi_{1-x}Tb_xFeO_3$ ($0\leq x\leq 0.2$) demonstrate phase transitions in the sequence of R3c ->Pbam ->Pnma and R3c ->Pnma for the La substituted and for the Tb substituted bismuth ferrite respectively. The difference sequences are attributed to their ionic sizes difference with the original bismuth ionic, which hampers the formation of stable Pbam structure in the $Bi_{1-x}Tb_xFeO_3$.

Thermal analysis was performed on the $Bi_{1-x}La_xFeO_3$ ($0\leq x\leq 0.2$) system. The peak corresponding to the Neel temperature is seen for every composition, peaks representing phase transition from R3c to Pnma and from Pbam to Pnma are displayed at $x\leq 0.1$ and x=0.2 respectively. However, for the x=0.15 and 0.175, the peak from R3c or Pbam to Pnma are overlapped and merged into one peak. Besides, Rietveld refinement was also carried out on the $Bi_{1-x}La_xFeO_3$ ($0\leq x\leq 0.2$) system. The weight fraction of rhombohedrally distorted structure R3c decreases with increase of the lanthanum content in the $Bi_{1-x}La_xFeO_3$ system.

Scopes of future work

Future work is still necessary, further investigation is suggested to be done based on,

1. Measurement of the nanoparticle size and distribution of synthesized ceramics by electric microscopic, and exploration of the relationship between the particle size and synthesis method.

2. Investigation on the B-site substituted bismuth ferrite, or substitution on both A site and B site are suggested to be investigated.

3. Comparison between various routes to make nanosized inorganic particles, search for the appropriate synthesis routes that can give desired compound with less impurity but enhanced electric and magnetic properties.

Acknowledgments

First of all, I would like to pay gratitude to my examiner, Professor Sten Eriksson, who believe me and offered me a chance of working at oxide group. I am also honored to have Christopher Knee as my supervisor, who was constantly keeping track of my work and giving me enormous valuable advice. I can honestly say that I would never have been able to accomplish my thesis work without the support from him.

I would also like to thank Stefan Norberg, Francis Kinyanjui and Habibur Rahman, who offered me instruction and guidance with great patience. And I really appreciate other people in the oxide group, their care and help always let me feel warm and happy.

Reference

1. I. E. Dzyaloshinskii, Sov. Phys. JETP 10, 628 (1960).
2. D. N. Astrov, Sov. Phys. JETP 11, 708 (1960).
3. V. J. Folen et al., Phys. Rev. Lett. 6, 607(1961)
4. Hans Schmid, Ferroelectrics 162, 317-338 (1994).
5. Daniel Khomskii Physics 2, 20 (2009).
6. A.M.Glazer, Acta Cryst. B28, 3384 (1972)
7. J. A. Bartkowska, International Journal of Thermophysics 32, 739 (2011).
8. Smolensky GA, Isupov VA, Agronovskaya AI, Sov Phys Solid State 1, 150 (1959).
9. Achenbach GD, James WJ, Gerson R, Am J. Ceram Soc. 50, 437 (1967).
10. Kubel F, Schmid H. Acta Crystallogr B 46, 698 (1990).
11. Spaldin, K. M. Rabe, M. Wuttig and R. Ramesh, Science 299, 1719 (2003).
12. A. K. Zvezdin, and D. Viehland, Appl. Phys. Lett. 84, 5261 (2004)
13. C. Ederer and N. A. Spaldin, Phys. Rev. B 71, 224103 (2005).
14. Ederer C, Spaldin NA. Phys Rev. B 71, 224103 (2005).
15. Mei Z. G, Shang S, Wang Y, Liu Z-K. Apply Phys. Lett. 98, 131904 (2011).
16. G. Catalan and J.F. Scott, Advanced Materials, 21, 2463 (2009).
17. A. G. Gavriliuk et al., Phase transition with suppression of magnetism in BiFeO3 at high pressure. Condensed Matter 4, Volume 82, 224 (2005).
18. a) Palemicz A. et al., Act Cryst. B 63: 537 (2007).
    b) Palemicz A. et al., Acta Phys. Pol. A 117, 296 (2010).
19. Scott JF. J Magn Magn. Mater. 321, 1689 (2009).
20. Catalan G, Scott JF. Adv Mater21, 2463 (2009).
21. Lebeugle JD, Colson D, Forget A, Viret M. Appl Phys. Lett. 91, 022907 (2007)
22. Wang J et al., Appl Phys. Lett. 85, 2574 (2004).
23. Eerenstein W et al., Science 307, 1203 (2005).
24. Chu YH et al., Appl Phys. Lett. 90, 252906 (2007)
25. Park TJ et al. Nano Lett.7, 766 (2007).
26. Sosnowska, T. Peterlin-Neumaier And E. Steichele J. Phys. C, Solid State Phys. 15, 4835 (1982).
27. J. R. Cheng, N, Li, and L. E. Cross, J. Appl. Phys. 94, 5153 (2003).
28. A. V. Zalesskii, A. K. Zvezdin, A. A. Frolov, and A. A. Bush, JETP Lett. 71, 465 (2000).
29 R.C Shannon Acta Cryst. A32, 751 (1976).

30. J. S. Kim, C. I. Cheon, C. H. Lee and P. W. Jang, J. Appl. Phys. 96, 468 (2004).
31. A Young Kim et al., Jonrnal of the Korean Ceramic society 4, 307 (2011).
32. B.Ruette, et al., Phys. Rev. B 69, 064114 (2004).
33. C. Ederer and N. A. Spaldn, Phys. Rev. B 71, 060401(R) (2005).
34. Palkar VR, Kundaliya DC, Malik SK. J. Appl. Phys. 93, 4337 (2003).
35. Palkar VR, Pinto R. Pramana, J. Phys. 58, 1003 (2002).
36. Ke H et al., J. Alloys Compd. 509, 2192 (2011).
37. G. Gogotsi, V. Galenko, B. Ozerskii, and N. Orlovskaya, Refract. Ind. Ceram. 42, 341 (2001).
38. D.A.Rusakovet al., Chem.Mater. 23, 285 (2011).
39. S. Karimi, I. M. Reaney, I. Levin, and I. Sterianou, Appl. Phys. Lett. 94, 112903 (2009)
40. S. Karimi, I. M. Reaney, Y. Han, J. Pokorny and I. Sterianous, J. Mater. Sci. 44, 5102 (2009).
41. D. C. Arnold, K. S. Knight, F. D. Morrison, P. Lightfoot, Phys. Rev. Lett. 102, 027602 (2009).
42. I. O. Troyanchuk et al., Phys. Rev. B 83, 054109 (2011).
43. G. Catalan et al., Phys. Rev. B 79, 212415 (2009).
44. G. Gogotsi, V. Galenko, B. Ozerskii, and N. Orlovskaya, Refract. Ind. Ceram. 42, 341 (2001).
45. S. Saxin and C. S. Knee, Dalton Trans. 40, 3462 (2011).